PAPER

Grain boundary passivation as an optimal strategy for perovskite solar cells with improved stability

Received 00th January 20xx,
Accepted 00th January 20xx

DOI: 10.1039/x0xx00000x

Yin Li[a], Hongbo Mo[a], Jingbo Wang[a], Zhengtian Yuan[a], Yanling He[b], Tao Zhu[c], Xiaoxue Fan[d], Gang Li[d], Jasminka Popović[e] and Aleksandra. B. Djurišić[a,*]

High performance perovskite solar cells have been obtained for a variety of different perovskite compositions. Here we investigate the stability of different perovskite compositions which can yield efficient solar cells under exposure to different stressors: illumination (with oxygen or humidity), and elevated temperature. Sensitivity of the perovskite to the exposure to different stress factors was strongly dependent on its composition, and stability-composition-efficiency dependences were complex. Nevertheless, MA-free perovskite clearly exhibits superior thermal stability and stability under illumination in oxygen, but exhibit sensitivity to moisture. We then investigate the effect of common strategies for stability improvement, namely additives for defect passivation, hydrophobic additives, and cross-linking additives, on the stability of MA-free perovskite, and achieved significant enhancement of stability with cross-linking additives. As cross-linking additives can hinder both ion migration under illumination as well as moisture ingress into the perovskite, they can facilitate superior stability compared to simple hydrophobicity enhancement. While all the additives resulted in similar efficiencies (~22%), cross-linking additives resulted in ~1.7 times increase in T_{80} compared to control devices during open circuit stability tests in ambient air with relative humidity 70%.

1. Introduction

The stability of lead halide perovskite materials and devices has been attracting increasing attention[1-6] as one of the major concerns for their commercialization. Commonly used lead halide perovskite materials have a formula $APbX_3$, where A denotes small organic cation, (methylammonium (MA) or formamidinium (FA)) or Cs^+, and X denotes halide anion.[1-6] These materials are known to be intrinsically unstable, and to degrade under exposure to illumination, elevated temperature, ambient environment (humidity, oxygen), and electrical bias,[1,5] which has led to the development of distinct device stability testing protocols aiming towards improved understanding of the degradation mechanisms.[5] Consequently, the perovskite material and/or device degradation upon exposure to humidity,[7-10] increased temperature,[11-19] illumination,[17,20-27] and bias[25,28-32] has been extensively studied, and a variety of different perovskite compositions have been investigated for improving efficiency and/or stability.[9,20,21,26,33-40]

While the device degradation occurs not only due to degradation of the perovskite layer, but also due to instabilities in charge transport layers and/or electrodes,[3-5] the stability of the perovskite layer and in particular confinement of the mobile ions to the perovskite layer and the prevention of the loss of volatile decomposition products is critical for improving the perovskite stability. However, the response to different stressors and dominant degradation mechanisms are highly dependent on the perovskite composition, including both anions and cations. For example, the stability of lead halide perovskites was found to be dependent on the halide anion, typically following I<Br<Cl stability trend.[1] Accordingly, increasing Br content was reported to contribute to improved tolerance to humidity, while in the case of illumination in the presence of oxygen, only pure $MAPbBr_3$ was stable.[34] However, while better stability with Br has been reported in some studies,[17,19,34] in others the presence of Br contributed to faster degradation[26] and Br incorporation was reported to lead to differences in phase transformations with increased temperature which can worsen thermal stability.[35] However, for a different (triple cation) composition, it was shown that both combination of three cations and incorporation of bromide plays a role in preventing undesirable phase transformations[36] and improves stability.[19,36]

In addition to anions, cations also affect the stability, with different cations resulting in different stability problems. For example, $FAPbI_3$ and $CsPbI_3$ exhibit crystal structure instabilities, where the black cubic/quasi-cubic phase transforms into undesirable thermodynamically stable yellow phase (δ-phase) upon exposure to heat, light, or humidity.[1,4,8] In

[a] Department of Physics, The University of Hong Kong, Pokfulam Road, Hong Kong SAR, China.
[b] Material characterization and preparation facility, The Hong Kong University of Science and Technology (Guangzhou), No.1 Duxue Road, Dongchong Town, Nansha District, Guangzhou, Guangdong Province, China
[c] Department of Electrical and Electronic Engineering, Research Institute for Smart Energy (RISE), The Hong Kong Polytechnic University, 11 Yuk Choi Rd, Hung Hom, Hong Kong SAR, China.
[d] Dept. of Mechanical Engineering, The University of Hong Kong, Pokfulam Road, Hong Kong SAR, China
[e] Ruđer Bošković Institute, Bijenička 54, 10000 Zagreb, Croatia
† Electronic supplementary information (ESI) available.

contrast, MA^+ cation readily decomposes under different conditions, contributing to general instability of MA-containing perovskites.[1] In terms of thermal stability, $CsPbI_3$ exhibited significantly higher activation energy for thermal degradation compared to hybrid organic-inorganic perovskites,[11] and MA-based and FA-based perovskites exhibited release of different gases upon thermal decomposition.[11] This likely occurs since for both MA and FA, in addition to reversible acid-base reaction involving deprotonation of organic ammonium and formation of HX acid, other irreversible reactions can occur.[11,12] In addition, MA exhibits worse thermal stability than FA,[13,33] and consequently MA-free perovskites exhibit better thermal stability than MA-containing perovskites[16,38] and residual MA^+ in the perovskite produced with MACl can still contribute to decreased stability.[33] Furthermore, thermal decomposition of CsFAMA perovskite was found to release MA^+- and I^--containing products, while Cs^+, FA^+ and Br^- were not affected.[14]

Differences in perovskite composition also affect response to humidity exposure. For example, upon exposure to humidity $MAPbI_3$ at first forms hydrated phases, followed by irreversible degradation to PbI_2, with the loss of volatile decomposition products (methylamine and HI),[3,4,7,10] while phase transformations occur for $FAPbI_3$ and $CsPbI_3$.[1,4,8] Degradation mechanisms under illumination in the presence of oxygen are also different for different perovskites, but they share some common features. In the presence of oxygen, photogenerated electrons from the perovskite are scavenged forming a superoxide ions[3,6,27] resulting in an excess of photogenerated holes.[27] Furthermore, under illumination photogenerated carriers participate in redox reactions, which result in the generation and recombination of different defects, which in turn can facilitate ion migration,[3,6] and which are accelerated by the exposure to oxygen[20,21] or moisture.[21] These reactions include oxidation of I^- by the photogenerated holes, and the reduction of cations (lead and/or organic cations).[20] However, these reactions in hybrid organic-inorganic perovskites would result in decomposition of the organic cation and the loss of volatile deprotonated amine, while in inorganic perovskites, Cs and Pb oxides are formed in addition to I_2 molecules.[4] The loss of volatile degradation products from the organic cation reduction makes the degradation irreversible,[29] in agreement with the report that degradation of perovskite occurs when not only halide anions but also organic cations participate in redox reactions.[32]

To date, various lead halide perovskite mixed compositions have exhibited improved stability compared to the most-studied $MAPbI_3$. However, contradictory reports exist in the literature on the stability effects of different mixed perovskite compositions, such as those including of MA and Br. For example, both worsening[26.35] and improving[17,19,36] of the perovskite stability with inclusion of Br has been reported. On the other hand, MA-free perovskites can exhibit advantage over MA-containing in terms of thermal stability and photostability, but not necessarily for stability under bias,[2] and can be susceptible to moisture.[8] In addition, scarcity of detailed multi-stressor studies and consideration of compositions which do not necessarily yield high performance devices with power conversion efficiency (PCE)>20%, as well as differences in perovskite fabrication and stability testing procedures, make it difficult to combine results from different studies to optimize perovskite composition. Consequently, an optimal perovskite composition which would result in superior stability with respect to illumination, moisture, and elevated temperature is not fully clear.

As the combination of stress factors can accelerate the degradation,[15] it is important to perform a comprehensive investigation of the effect of different stress factors on the stability of perovskite films with different compositions, as well as examine different passivation methods for improving the stability. Therefore, we investigated the following perovskite compositions: commonly used CsFAMA triple cation perovskite with composition $Cs_{0.03}(FA_{0.83}MA_{0.17})_{0.97}Pb(I_{0.83}Br_{0.17})_3$,[41,42] low-Br perovskite ($Cs_{0.05}(FA_{0.98}\ MA_{0.02})_{0.95}Pb(I_{0.98}Br_{0.02})_3$)[43] and MA-free perovskite $Cs_{0.1}FA_{0.9}PbI_{2.9}Br_{0.1}$.[44] We find that MA-free perovskite exhibits the best stability among the compositions under all testing conditions, and that this perovskite composition is still sensitive to exposure to moisture under illumination. To elucidate what type of passivating agent would yield most significant improvement in the stability, we then investigated additives[45-50] with different functionality, i.e. additives which have different functional groups for passivating defects, increasing hydrophobicity, as well as cross-linking grains. The effects of these additives on the perovskite film and device stability are discussed.

It should be noted that device stability remains a major problem for perovskite solar cells. To tackle the problem of practically relevant stability, it is important to both address the perovskite and device design (perovskite composition, additives, selection of charge transport layers and electrodes), as well as encapsulation.[51,52] Different encapsulation methods have been proposed for individual cells and modules,[51,52] which can serve the function of preventing ingress of oxygen and moisture into the device package, prevent outgassing of volatile perovskite decomposition products, as well as prevent leakage of lead. For the purpose of commercialization of perovskite devices, it is also important to develop appropriate accelerated aging protocols,[53-58] which can also be combined with different spectroscopic investigations of the degradation processes.[55,57]

Acceleration of the degradation could be achieved by different protocols, such as increased illumination intensity,[53] or increased temperature under illumination.[54] Among different acceleration laboratory testing protocols, illumination at elevated temperatures has been linked to outdoor testing performance.[54] In general, it has been proposed that combinations of different testing protocols involving multiple associated stressors needs to be employed for prediction of outdoor stability,[54,55] since degradation signatures for outdoor testing could not be reproduced by a single-stressor test (UV illumination, thermal cycling).[55] In addition, linking the results of indoor accelerated testing to outdoor performance is further complicated by the fact that observed degradation processes, such as partial delamination, can be climate dependent.[56] In addition, while acceleration factors considering diffusion of oxygen into the package have been derived, but the barriers

designed to confine volatile perovskite degradation components have not been considered.[58]

In this work, we employed testing without encapsulation as accelerated aging, since we aim to investigate the relationships between changes in perovskite films exposed to different stressors and the device stability. We have tested unencapsulated devices to accelerate degradation,[59] as we commonly observe the same stability trends in devices with and without encapsulation, just with longer T_{80} with encapsulation. This indicates that the processes contributing to the degradation cannot be entirely suppressed by encapsulation preventing ingress of oxygen and moisture, as well as preventing loss of volatile decomposition products. As the halide oxidation is driven by excess photogenerated holes,[27] this process can occur even in the absence of oxygen acting as an electron scavenger. Consequently, it is important to improve the stability of the devices as much as possible through perovskite composition and device architecture optimization, to ensure that optimized devices would exhibit exceptional stability combined with encapsulation.

2. Results and Discussion

Figure 1 shows the J-V curves for champion devices for 3 different compositions investigated. We can observe that for all compositions we obtain high performance devices, with the lowest efficiency ~22% obtained for CsFAMA perovskite, while we obtain higher efficiency (close to 24%) for low-Br perovskite, and 22-23% for MA-free perovskite, which is the only composition exhibiting obvious hysteresis, indicating that further optimization of charge extraction in these devices is possible.

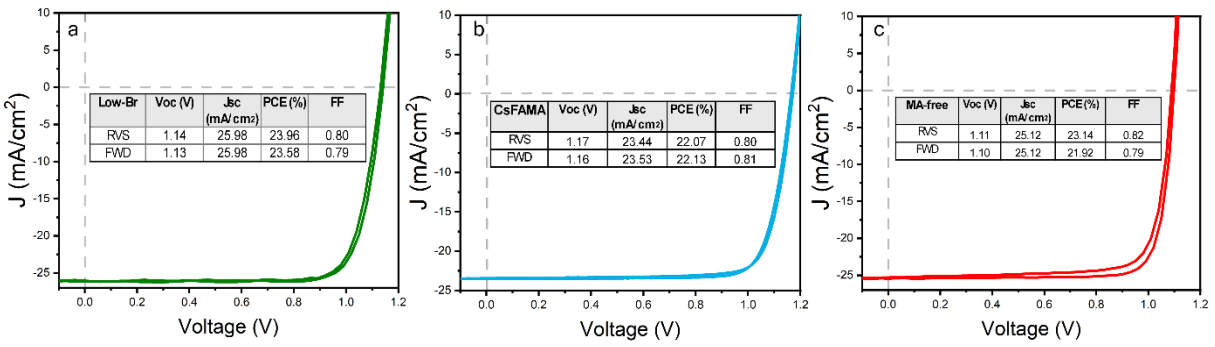

Figure 1 J-V curves (forward and reverse scan) of champion devices for three different perovskite compositions.

However, while low-Br perovskite yields the highest efficiency, this composition exhibits very poor stability, as shown in **Figure 2**. Low-Br perovskite crystallizes in the cubic space group *P*4-3*m*, with refined unit-cell parameter a = 6.329(4) Å, similar to the previously reported structure.[60] Exposure in all conditions leads to the degradation of the cubic phase, as evidenced by the appearance of PbI_2 diffraction lines, while the illumination additionally causes the appearance of both hexagonal δ-(FA)PbI_3 phase in $P6_3mc$ space group with unit-cell parameters a = 8.624(1) Å, c = 7.906(6) Å as reported by Kanatzidis *et. al.*[61] and orthorhombic δ-$CsPbI_3$ phase in *Pnma* space group with refined unit-cell parameters a = 10.445(5) Å, b = 4.798(1) Å and c = 17.759(4) Å.[61] Along with the decrease of intensities of diffraction lines during aging in all conditions, from profile fitting analysis we can also observe pronounced broadening of perovskite diffraction lines indicating the deterioration in overall perovskite crystallinity (**Figure S1a**).

CsFAMA perovskite has also been refined in *P*4-3*m* space group with unit-cell parameter a = 6.282(6) Å. Observed decrease of mixed perovskite unit-cell parameter compared to low-Br is in accordance with the chemical composition since this perovskite sample contains smaller amount of FA cation (which is the largest cation among MA and Cs, with effective ionic radius r = 253 pm thus having the biggest effect on the size of the unit cell). Unlike low-Br, for mixed perovskites aging in all conditions leads to the appearance PbI_2 exclusively, without crystallization of δ-(FA)PbI_3 or δ-$CsPbI_3$ phases, similar to the degradation of perovskites which contain only MA cations.[3,4,7,10,17] As in the case of low-Br, degradation of mixed composition is also accompanied with severe loss of crystallinity (**Figure S1b)**. It should be noted that the degradation under illumination which leads to the formation of PbI_2 is a consequence of photo/electrochemical degradation processes initiated by halide oxidation.[59,62,63] In contrast, degradation involving phase transformations has not been directly linked to photo/electrochemical degradation.

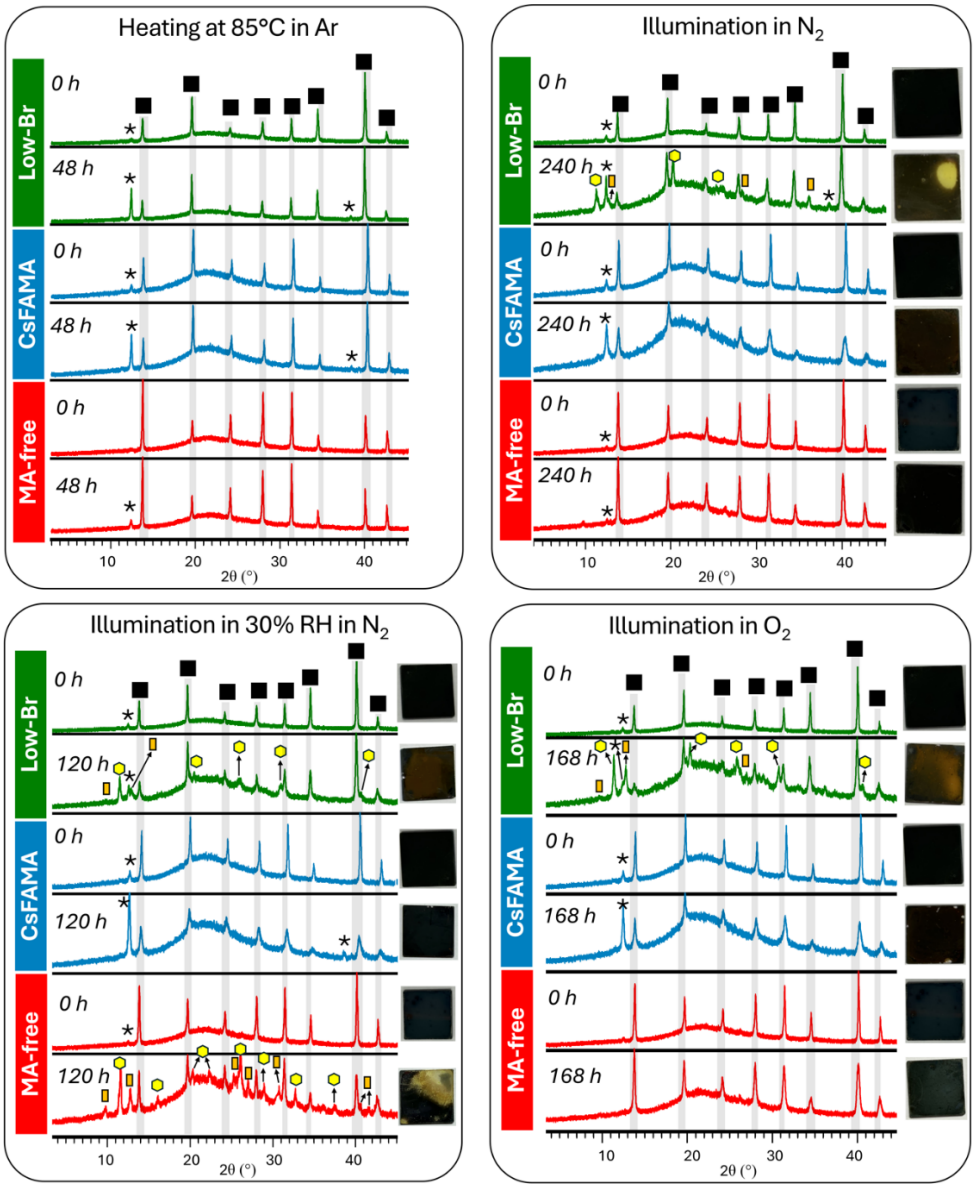

Figure 2. XRD patterns of low-Br, CsFAMA, and MA-free perovskite films before and after exposure to different aging conditions. Cubic perovskite phase is denoted by black squares while the reflection positions of hexagonal δ-(FA)PbI_3 and orthorhombic δ-$CsPbI_3$ phases are denoted with yellow hexagons and orange rectangles, respectively. The insets show photos of the films.

Finally, MA-free perovskite, refined in cubic space group with unit cell parameter a = 6.3189(1) Å, exhibits excellent stability under all conditions (just a small increase in PbI_2 is observed for aging at 85°C) which is in agreement with improved thermal stability[2,38] and photostability[2] of MA-free perovskites.[38] Stability of MA-free perovskites is most affected by the presence of moisture where we observe the appearance of both δ-(FA)PbI_3 or δ-$CsPbI_3$ phases. Results of refinement for MA-free perovskite after aging under illumination the N_2 in the presence of moisture are shown in **Figure S2**. It is interesting to notice that, unlike low-Br and mixed perovskites, degradation of MA-free perovskite does not seem to have significant effect on its overall crystallinity; we can observe that full-width-at-half-maxima parameter for aged sample remains almost the same as in the as-prepared indicating there is no decrease of coherent diffraction domains (crystallites) and no significant loss of crystallinity (**Figure S1c)**. Similar stability trends, with MA-free perovskite exhibiting the highest stability, are also observed under illumination in ambient air.[59]

PAPER

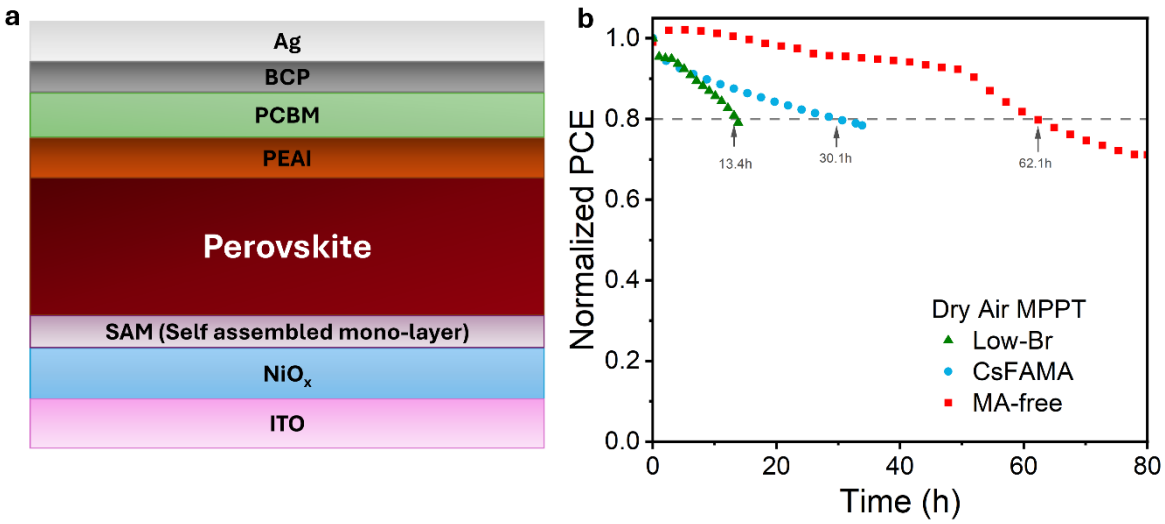

Figure 3. a) Schematic diagram of the device structure and b) Normalized PCE vs. time under simulated solar illumination 100 mW/cm^2 in dry air.

In addition to inferior stability, low-Br perovskite is also highly sensitive to the glove box temperature, as illustrated in **Figure S3**. Among the three compositions, CsFAMA perovskite exhibits the lowest variation of device performance with the glove box temperature, as expected from widespread use of this particular perovskite composition. To verify whether the trends observed in film stability are preserved in the device stability comparisons, device stability tests were conducted following ISOS-L-1 protocol[5] without encapsulation in dry air and under open circuit (OC) conditions to accelerate degradation.[31] Schematic diagram of the device architecture and the obtained results of the stability tests are shown in **Figure 3**. Significantly higher stability of MA-free perovskite is obtained compared to other compositions. As the $MAPbI_3$ has inferior photostability compared to other perovskite compositions[21] and its degradation produces highly volatile degradation products,[23] and the loss of volatile decomposition products and consequently irreversible degradation,[29] it is expected that MA-containing perovskites would exhibit worse stability compared to MA-free composition.

To address the sensitivity of MA-free perovskite to humidity exposure without introducing complex processing protocols, we considered different additives, with chemical structure shown in **Figure S4**. While the need for the investigation of the effect of perovskite compositions and additives on photoelectrochemical processes, ion migration, and degradation has been recognized, the effect of additives targeting point defect passivation or more general grain boundary passivation is largely unknown. A number of different additives with various functionalities has been investigated in the literature.[45-50,64,65] Here we selected different additives, which have some similarities, while each has one distinct feature. 3-phosphonopropionic acid (3PPA) was reported to modulate the crystallization to increase the grain size, release residual strain, and passivate grain boundary defects.[50] For this additive, C=O and P=O bonds can coordinate with Pb^{2+} and form hydrogen bonds with N-H group of organic cation.[50] Thus, the presence of multiple functional groups in this additive allows interactions with lead ions through coordination or ionic bonding, as well as organic and halogen ions through hydrogen bonding.[50] Phosphonic group in particular is expected to be beneficial due to its stronger H-donating character.[49,50] Moreover, 3PPA was reported to passivate shallow defects (FA and I vacancies) which affect the device stability.[49] We also considered formamidinium tetrafluoroborate ($FABF_4$), since BF_4^- was proposed to regulate perovskite crystallization dynamics,[45] passivate halogen vacancies,[45,46] increase hydrophobicity[45] and reduce trap density.[47] In general, organic

cation-pseudohalide compounds can suppress the formation of both cation and anion vacancies.[45,46,65] For example, in the case of $FABF_4$, BF_4^- would fill halide vacancies,[45-47]since BF_4^- can be effectively incorporated into the lattice of a mixed halide perovskite.[47] Finally, we also investigated the use of cross-linkable (CL) additive, *N*,*N*-Methylenebisacrylamide, which has been shown to significantly improve photostability of perovskite films and suppress expulsion of iodide under illumination at elevated temperature.[48] It was also proposed to suppress ingress of moisture into the perovskite and leakage of Pb out of the perovskite.[48] This additive is also capable of interacting with under-coordinated Pb^{2+} through C=O group, as well as the formation of hydrogen bonds through N-H group.[48] In addition, this additive forms an uniform amorphous layer on the surface of perovskite grain.[48] It should be noted that the passivation of grain boundaries and interfaces is particularly important, as the dangling bonds and disorder are expected to provide abundant reactive sites for photoelectrochemical reactions leading to perovskite degradation, in addition to providing pathways for ion migration.[63] Thus, all additives investigated can passivate defects and form hydrogen bonds with the perovskite. Hydrogen bonding is considered particularly significant as it facilitates surface hydrophobicity and self-healing.[65] The encapsulation of individual grain with a thin polymer layer[48] is a distinguishing feature of CL additive compared to other additives investigated. In the case of 3PPA, stronger hydrogen bonding through phosphonic group is a distinguishing feature, while for $FABF_4$ we expect to see increased resistance to moisture due to increased binding energy of H_2O due to elimination of cation and anion vacancies typical for organic ammonium-pseudohalide salt passivators.[64]

We can observe that all additives result in increased hydrophobicity of the perovskite film, as shown in **Figure S5**, with the contact angles observed exhibiting order Control<$FABF_4$<CL<3PPA. Despite the fact that additives can alter the perovskite crystallization, no significant change in the morphology is observed, as shown in **Figure S6**. From FTIR measurements of films containing additives and FAI (**Figure S7**) and additives and perovskite (**Figure S8**) we can observe peak shifts as well as changes in relative peak intensities and consequent changes in peak shapes for peaks corresponding to N-H stretches, C=N stretch and N-H bending,[50,66] indicating changes in hydrogen bonding with organic cations.[50] This is not surprising as all additives contain functional groups capable of forming hydrogen bonds. The most prominent changes have been observed for CL additive.

To evaluate the effects of additives on resistance to humidity, the perovskite films were aged in ambient atmosphere (RH=70%) and obtained results are shown in **Figure 4**. Based on the intensities of perovskite diffraction lines after 480 of aging, we can observe improved stability for all additives compared to the control. However, CL and $FABF_4$ are clearly being more effective than 3PPA in spite of their lower hydrophobicity compared to 3PPA (**Figure S5**). Elimination of surface cation and anion vacancies expected for $FABF_4$ is expected to decrease interaction with H_2O,[64] while for CL surface encapsulation of perovskite grains by CL is likely responsible for the improved stability. It should also be noted that the dominance of δ-(FA)PbI_3 phase is associated with significant decrease in the perovskite phase, while the presence of similar levels of δ-(FA)PbI_3 and δ-$CsPbI_3$ phases is associated with the persistence of the perovskite phase.

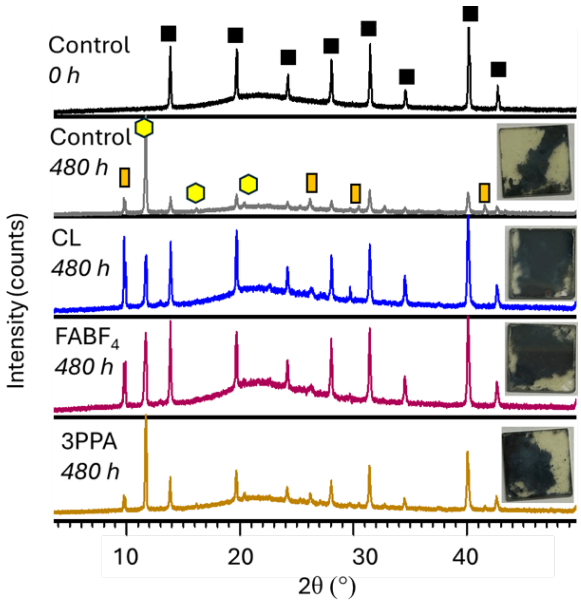

Figure 4. XRD patterns of MA-free perovskite films with different additives before and after aging in ambient environment (~70% RH) under ambient illumination for control, CL, $FABF_4$, and 3PPA. Cubic perovskite phase is denoted by black squares while the

reflection positions of hexagonal δ-(FA)PbI_3 and orthorhombic δ-$CsPbI_3$ phases are denoted with yellow hexagons and orange rectangles, respectively.

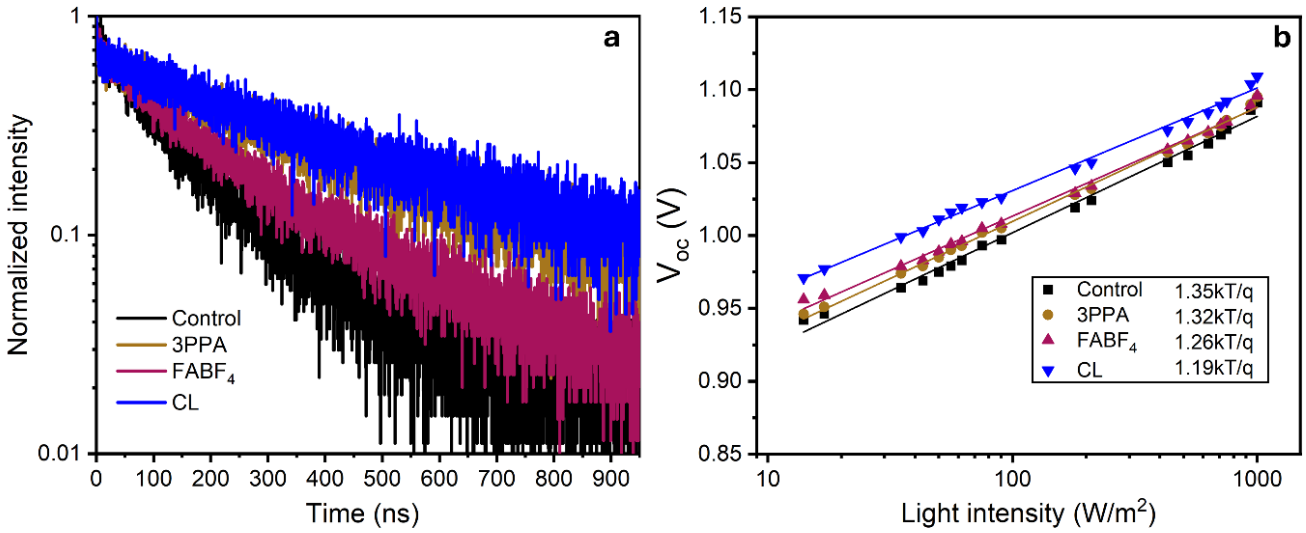

Figure 5. a) TRPL decay curves of perovskite films with different additives b) V_{oc} as a function of illumination power for solar cells with different additives.

To investigate the effects of different additives of defect passivation, TRPL measurements were performed. This technique is commonly used for the investigation of charge transfer and/or recombination in halide perovskites,[67,68] but the interpretation of the obtained data can be difficult due to influence of the model used[67] as well as the sample quality and measurement parameters[68] on the obtained results. As the films exhibit no significant morphology differences (**Figure S6**), they are expected to have similar quality and hence the TRPL measurements can serve as useful tool for relative comparisons between these samples. To enhance the analysis of the measurement results shown in **Figure 5a**, both bi-exponential decay model and bimolecular trapping-detrapping model[67] were used for fitting and the obtained parameters are summarized in **Table S1** and **S2**, respectively. Bi-exponential model is commonly used for fitting the TRPL data of lead halide perovskite materials, with shorter decay time attributed to trap mediated recombination and longer decay time to radiative recombination.[67] However, for all the additives we can observe a significant decrease in the shorter decay time and a significant increase in the longer decay time. As such a simplistic model is often difficult to interpret with multiple processes contributing to each of the two decay times, we also analyzed the data using bimolecular trapping-detrapping model.[67] We can observe that there is a small increase in bimolecular recombination and a corresponding decrease in trap-mediated recombination for all three additives compared to control samples, but the effect is small for 3PPA and $FABF_4$, while more pronounced change is observed for CL additive. This observation is consistent with the decrease in the diode ideality factor n_{ID} determined from V_{oc} vs. illumination power dependence (**Figure 5b**), which is consistent with a decrease in trap-assisted recombination.[49] Similar to a previous report for different perovskite composition, 3PPA resulted in a very small decrease in the ideality factor compared to control sample, as expected since hydrogen bond formation involving shallow defects is not expected to affect non-radiative recombination.[49] The most significant difference was obtained for CL additive, which also exhibited the lowest concentration of the trap states N_T from the TRPL data. For the CL additive, we also observe higher V_{oc} and narrower V_{oc} distribution compared to other samples (**Table S3**, **Figure S10**), in agreement with TRPL and n_{ID} measurements. Lower ideality factor and the reduction of non-radiative recombination in the case of CL is in agreement with the previous report for $MAPbI_3$ with CL.[48]

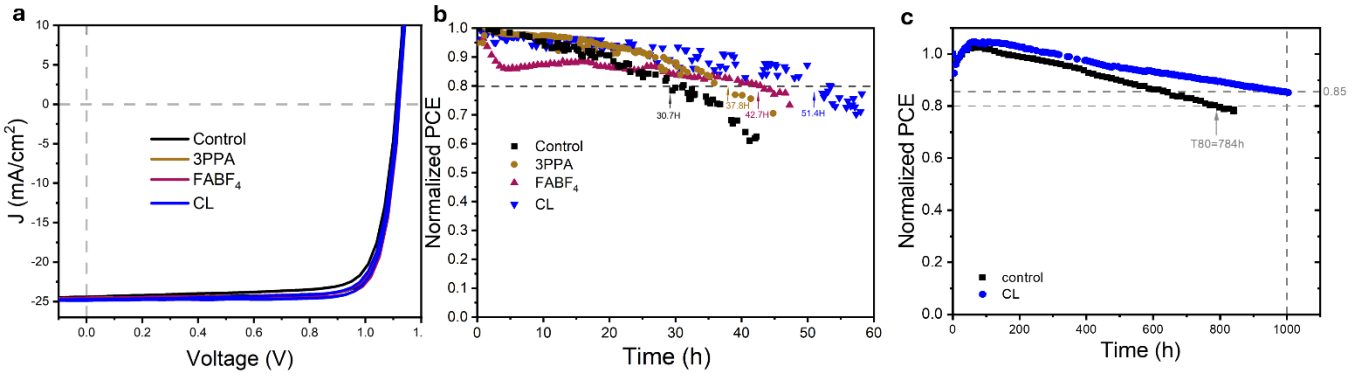

Figure 6. a) J-V curves for solar cells with different additives. b) Normalized PCE of devices without encapsulation under simulated solar illumination (100 mW/cm^2) MPPT in ambient (~70% RH) c) Normalized PCE of encapsulated devices under simulated solar illumination (100 mW/cm^2) MPPT in ambient (~70% RH) (ISOS-L-1).

The J-V curves of solar cells with different additives are shown in **Figure 6a**, while corresponding external quantum efficiency (EQE), stabilized power output (SPO), and device performance statistics are shown in **Figure S9** and **S10**. Device performance statistics (12 devices from 4 substrates) is also summarized in **Table S3**. No significant reproducibility differences were observed between control samples and devices with different additives, as any failures observed and excluded from statistical analysis have obvious defects, such as dust particles, clearly observable by naked eye. It should be noted that devices with CL additive demonstrated smaller performance variation from device to device, as observed in device performance statistics in **Figure S10**, as well as small difference in J-V curves between the best and the worst devices, shown in **Figure S11.** All the additives yield some improvement in the best device performance, but overall the differences between the control device and devices with additives are small. However, significant differences in device stability are obtained, as shown in **Figure 6 b** and **6c**. It has been previously shown that 3PPA can passivate shallow defects and thus improve device lifetime, without having a significant effect on the efficiency.[49] As the previous investigation was applied to RbCsFAMA and CsFAMA perovskite and conventional architecture devices,[49] and we investigated MA-free perovskite in inverted architecture, the shallow defect passivated by 3PPA is likely not cation related. We can also observe that $FABF_4$ and 3PPA result in a small increase in FF, and a small decrease in V_{oc}, while for CL the opposite trend is observed. This indicates a possible difference in types of shallow defects targeted by different additives. It has been previously shown that 3PPA can passivate one of the three defects present in RbCsFAMA perovskite, namely the most shallow defect.[49]

In terms of device stability, the most significant improvement is obtained for CL additive. The obtained results highlight critical role of cross-linkable grain boundary passivation, which simultaneously slows down the ingress of oxygen and moisture into the perovskite and reduces ion migration through the grain boundaries. Our results also highlight the critical importance of perovskite composition, since in our case 3PPA did not yield as significant stability enhancements as previously reported for RbCsMAFA devices[49] or MA-free devices with different composition.[50] It should also be noted that defects in perovskite are constantly being generated and are annihilated under illumination and/or bias as a consequence of electrochemical redox reactions in the perovskite.[63] Consequently, the device degradation is strongly affected by the migration of oxidized iodide species, rather than simply determined by initial concentration of native defects present. Considering that the cross-linkable stabilization strategies rely on reducing migration of mobile ions as well as ambient air molecules through the grain boundaries instead of passivation of specific types of defects) whose concentration is perovskite composition dependent, we expect that cross-linking strategies can yield more universal stability improvements compared to simple defect passivation.

To distinguish between the suppression of ion migration, confinement of degradation products, and/or suppression of moisture and oxygen ingress, we performed aging under illumination in ambient, and examined the perovskite crystal structure and composition after the aging. J-V curves of the cells before and after aging in ambient under open circuit condition under 1 Sun illumination are shown in **Figure S12**, while the corresponding XRD patterns are shown in **Figure S13** and Pb and I content in the perovskite after removal of the electrode and PCBM is summarized in **Table S4**. Control devices have worse stability and fail sooner than the devices with additives, so that representative J-V curve for control device is shown for 48 h, while for others it is 72 h, and the perovskite film analysis is performed after 72 h in all cases. We can observe increased hysteresis in J-V curves after aging (**Figure S12**). Ionic losses are known to be a significant contributor to performance degradation under illumination,[69] and they typically manifest via significant reduction in J_{sc}, as we can indeed observe in our devices. Reduction of FF, but lower hysteresis in aged devices compared to other additives is observed for 3PPA, while CL devices consistently exhibit the best stability consistent with

stability tests under MPPT (**Figure 6b**). The presence of hysteresis in perovskite solar cells aged in ambient has been linked to moisture/O_2 ingress and changes in iodide distribution,[70] and 3PPA samples exhibited the highest hydrophobicity. However, EDX analysis exhibits only minor differences in Pb:I ratios before and after aging for all samples. Possible explanation for this is the fact that EDX was performed in another university, which could have reversed the changes due to ion migration as the samples were not illuminated during transport. It is generally known that ion migration is responsible for the reversible performance losses during day/night cycling,[71] and that the degradation of the perovskite can be reversible if the oxidized iodine is still present in the material, and become irreversible upon expulsion of oxidized iodine.[62] From the XRD patterns (**Figure S13**), we can observe degradation in the perovskite crystallinity for all samples except CL sample, but no additional phases could be observed for the test time used which lead to significant degradation of solar cell performance. Thus, the mobile ions originating from photo/electrochemical redox reactions at the surface of perovskite grains[63] likely resulted in crystallinity degradation of control, 3PPA, and $FABF_4$ samples. In contrast, as CL additive covers individual perovskite grains with very thin amorphous polymer layer,[48] we can attribute increased stability to the grain boundary stabilization as there is negligible change in the intensity of XRD peaks.

3. Conclusion

We investigated the effect of perovskite composition to its degradation in different environments under illumination. We found different dominant degradation pathways (degradation to PbI_2 in CsFAMA perovskite, degradation to undesirable crystal structures in other compositions) depending on the perovskite composition. While MA-free perovskites exhibited better stability overall, they were sensitive to humidity exposure under illumination. Among different passivating molecules, cross-linking passivator exhibited more significant improvement in device stability compared to passivators which only had defect passivating capability. Our results clearly demonstrate that internal encapsulation of perovskite grains by cross-linking additive is of critical importance in achieving improved long term stability.

Author contributions

Yin Li: conceptualization, formal analysis, investigation, methodology and writing-review & editing. Hongbo Mo, Jingbo Wang, Zhengtian Yuan: investigation. Yanling He: investigation. Tao Zhu: investigation. Xiaoxue Fan: investigation. Gang Li: supervision. Jasminka Popović: conceptualization and formal analysis. Aleksandra. B. Djurišić: conceptualization, writing-original draft, writing-review & editing and supervision.

Conflicts of interest

The authors declare that they have no competing financial interests.

Data availability

The data supporting this article have been included as part of the Electronic Supplementary Information.

Acknowledgements

This work was supported by the RGC CRF project 7018-20G and Seed Funding for Basic Research and Research Output Award of the University of Hong Kong. The authors would like to acknowledge Li Wei from Department of Mechanical Engineering, The University of Hong Kong for contact angle measurements.

Notes and references

1 B. W. Park, S. I. Seok, *Adv. Mater.* **2019**, *31*, 1805337.
2 X. Meng, X. Tian, S. Zhang, J. Zhou, Y. Zhang, Z. Liu, W. Chen, *Solar RRL* **2022**, *6*, 2200280.
3 J. Zhuang, J. Wang, F. Yan, *Nano-Micro Lett*. **2023**, *15*, 84.
4 W. Chi, S. K. Banerjee, *Chem. Mater. 2021*, 33, 4269.
5 M. V. Khenkin, E. A. Katz, A. Abate, G. Bardizza, J. J. Berry, C. Brabec, F. Brunetti, V. Bulović, Q. Burlingame, A. Di Carlo, R. Cheacharoen, Y. B. Cheng, A. Colsmann, S. Cros, K. Domanski, M. Dusza, C. J. Fell, S. R. Forrest, Y. Galagan, D. Di Girolamo, M. Grätzel, A. Hagfeldt, E. von Hauff, H. Hoppe, J. Kettle, H. Köbler, M. S. Leite, S. F. Liu, Y. L. Loo, J. M. Luther, C. Q. Ma, M. Madsen, M. Manceau, M. Matheron, M. McGehee, R. Meitzner, M. K. Nazeeruddin, A. F. Nogueira, Ç. Odabaşı, A. Osherov, N. G. Park, M. O. Reese, F. De Rossi, M. Saliba, U. S. Schubert, H.J. Snaith, S. D. Stranks, W. Tress, P. A. Troshin, Vida Turkovic, S. Veenstra, I. Visoly-Fisher, A. Walsh, T. Watson, H. Xie, R. Yıldırım, S. M. Zakeeruddin, K. Zhu, M. Lira-Cantu, *Nat. Energy* **2020**, *5*, 35.
6 M. U. Ali, H. Mo, A. U. Rehman, T. L. Leung, A. B. Djurišić, *Trends Chem.* **2024**, *6*, 248.
7 V. Nalini, G. N. Nagy, A. Rahaman, S. K. Kalpathy, T. Thomas, T. Sumangala, M. U. Kahaly, *Mater. Adv.* **2024**, *5*, 6426.
8 Y. Liu, Z. Wu, Y. Dou, J. Zhang, T. Bu, K. Zhang, D. Fang, Z. Ku, F. Huang, Y.-B. Cheng, *J. Phys. Chem. C* **2020**, *124*, 12249.
9 P. Raval, M. A. Akhavan Kazemi, J. Ruellou, J. Trébosc, O. Lafon, L. Delevoye, F. Sauvage, G. Manjunatha Reddy, *Chem. Mater.* **2023**, *35*, 2904.
10 B. P. Kore, M. Jamshidi, J. M. Gardner, *Mater. Adv.* **2024**, *5*, 2200.
11 E. J. Juarez-Perez, L. K. Ono, Y. Qi, *J. Mater. Chem. A* **2019**, *7*, 16912.
12 E. J. Juarez-Perez, L. K. Ono, I. Uriarte, E. J. Cocinero, Y. Qi, *ACS Appl. Mater. Interfaces* **2019**, *11*, 12586.
13 J. Song, W. Hu, X.-F. Wang, G. Chen, W. Tian, T. Miyasaka, J. Mater. Chem. A 2016, 4, 8435.
14 J. Yang, X. Liu, Y. Zhang, X. Zheng, X. He, H. Wang, F. Yue, S. Braun, J. Chen, J. Xu, *Nano Energy* **2018**, *54*, 218.
15 M. Bag, L. A. Renna, R. Y. Adhikari, S. Karak, F. Liu, P. M. Lahti, T. P. Russell, M. T. Tuominen, D. Venkataraman, *J. Am. Chem. Soc.* **2015**, *137*, 13130.
16 W. Tan, A. R. Bowring, A. C. Meng, M. D. McGehee, P. C. McIntyre, *ACS Appl. Mater. Interfaces* **2018**, *10*, 5485.
17 P.-C. Huang, T.-J. Yang, C.-J. Lin, M.-Y. Wang, W.-C. Lin, *Langmuir* **2024**, *40*, 11873.

18 P. Deng, W. Dai, Y. Gou, W. Zhang, Z. Xiao, S. He, X. Xie, K. Zhang, J. Li, X. Wang, *ACS Appl. Mater. Interfaces* **2024**, *16*, 29338.
19 M. Saliba, T. Matsui, J.-Y. Seo, K. Domanski, J.-P. Correa-Baena, M. K. Nazeeruddin, S. M. Zakeeruddin, W. Tress, A. Abate, A. Hagfeldt, Energ Environ. Sci. 2016, 9, 1989.
20 T. Sekimoto, R. Uchida, M. Hiraoka, T. Matsui, R. Kikuchi, T. Nakamura, T. Yamamoto, K. Kawano, T. Negami, Y. Kaneko, ACS Applied Energy Mater. 2022, 5, 4125.
21 K. Kwak, E. Lim, N. Ahn, J. Heo, K. Bang, S. K. Kim, M. Choi, *Nanoscale* **2019**, *11*, 11369.
22 N. H. Nickel, F. Lang, V. V. Brus, O. Shargaieva, J. Rappich, *Adv. Electron. Mater.* **2017**, *3*, 1700158.
23 X. Tang, M. Brandl, B. May, I. Levchuk, Y. Hou, M. Richter, H. Chen, S. Chen, S. Kahmann, A. Osvet, *J. Mater. Chem. A* **2016**, *4*, 15896.
24 A. Senocrate, T. Acartürk, G. Y. Kim, R. Merkle, U. Starke, M. Grätzel, J. Maier, *J. Mater. Chem. A* **2018**, *6*, 10847.
25 D. Bryant, N. Aristidou, S. Pont, I. Sanchez-Molina, T. Chotchunangatchaval, S. Wheeler, J. R. Durrant, S. A. Haque, *Energy Environ. Sci.* **2016**, *9*, 1655.
26 A. F. Akbulatov, M. I. Ustinova, L. Gutsev, S. A. Tsarev, N. N. Dremova, I. Zhidkov, S. Y. Luchkin, B. R. Ramachandran, L. Frolova, E. Z. Kurmaev, *Nano Energy* **2021**, *86*, 106082.
27 J. T. DuBose, P. V. Kamat, *Acc. Mater. Res*. **2022**, *3*, 761.
28 E. Zheng, Z. Niu, G. A. Tosado, H. Dong, Y. Albrikan, Q. Yu, *J. Phys. Chem. C* 2020, 124, 18805.
29 N. A. Emelianov, V. V. Ozerova, Y. S. Fedotov, M. V. Zhidkov, R. R. Saifutyarov, M. S. Malozovskaya, M. S. Leshchev, E. V. Golosov, L. A. Frolova, P. A. Troshin, *Materials* **2023**, *16*, 4277.
30 R. Singh, H. Hu, T. Feeney, A. Diercks, F. Laufer, Y. Li, T. Duong, F. Schackmar, B. A. Nejand, U. W. Paetzold, *ACS Appl. Mater. Interfaces* **2024**, *16*, 27450.
31 K. M. Anoop, M. V. Khenkin, F. Di Giacomo, Y. Galagan, S. Rahmany, L. Etgar, E. A. Katz, I. Visoly-Fisher, *Solar RRL* **2020**, *4*, 1900335.
32 Z. Xu, R. A. Kerner, J. J. Berry, B. P. Rand, *Adv. Funct. Mater*. **2022**, *32*, 2203432.
33 D. J. Tay, B. Febriansyah, T. Salim, M. Kovalev, A. Sharma, T. M. Koh, S. G. Mhaisalkar, J. W. Ager, N. Mathews, *Small* **2024**, *2403389*. DOI: 10.1002/smll.202403389
34 S. Pont, D. Bryant, C.-T. Lin, N. Aristidou, S. Wheeler, X. Ma, R. Godin, S. A. Haque, J. R. Durrant, J. Mater. Chem. A **2017**, *5*, 9553.
35 D. K. LaFollette, J. Hidalgo, O. Allam, J. Yang, A. Shoemaker, R. Li, B. Lai, B. Lawrie, S. Kalinin, C. A. Perini, *J. Am. Chem. Soc.* **2024**, *146*, 18576.
36 K. Wang, Q. Yao, J. Zhang, L. Jing, X. Cheng, C. Shang, C. Li, F. Chen, T. Zhou, H. Zhu, *Chem. Mater*. **2022**, *34*, 1179.
37 M. Bidikoudi, V. Dracopoulos, E. Stathatos, *Energy Adv.* **2022**, *1*, 76.
38 J. A. Schwenzer, T. Hellmann, B. A. Nejand, H. Hu, T. Abzieher, F. Schackmar, I. M. Hossain, P. Fassl, T. Mayer, W. Jaegermann, *ACS Appl. Mater. Interfaces* **2021**, *13*, 15292.
39 C. Yi, J. Luo, S. Meloni, A. Boziki, N. Ashari-Astani, C. Grätzel, S. M. Zakeeruddin, U. Röthlisberger, M. Grätzel, *Energy Environ. Sci.* **2016**, *9*, 656.
40 S. Wang, L. Tan, J. Zhou, M. Li, X. Zhao, H. Li, W. Tress, L. Ding, M. Graetzel, C. Yi, *Joule* **2022**, *6*, 1344.
41 M. Saliba, J.-P. Correa-Baena, C. M. Wolff, M. Stolterfoht, N. Phung, S. Albrecht, D. Neher, A. Abate, *Chem. Mater.* **2018**, *30*, 4193.
42 J. Lin, Y. Wang, A. Khaleed, A. A. Syed, Y. He, C. C. Chan, Y. Li, K. Liu, G. Li, K. S. Wong, *ACS Appl. Mater. interfaces* **2023**, *15*, 24437.
43 D. Li, Y. Huang, R. Ma, H. Liu, Q. Liang, Y. Han, Z. Ren, K. Liu, P. W. K. Fong, Z. Zhang, Adv. Energy Mater. 2023, 13, 2204247.
44 Q. An, L. Vieler, K. P. Goetz, O. Telschow, Y. J. Hofstetter, R. Buschbeck, A. D. Taylor, Y. Vaynzof, *Adv. Energy Sustainability Res.* **2021**, *2*, 2100061.
45 C. Su, R. Wang, J. Tao, J. Shen, D. Wang, L. Wang, G. Fu, S. Yang, M. Yuan, T. He, *J. Mater. Chem. A* **2023**, *11*, 6565.
46 L. Yang, X. Ma, X. Shang, D. Gao, C. Wang, M. Li, C. Chen, B. Zhang, S. Xu, S. Zheng, *Solar RRL* **2021**, *5*, 2100352.
47 J. Zhang, S. Wu, T. Liu, Z. Zhu, A. K. Y. Jen, *Adv. Funct. Mater*. **2019**, *29*, 1808833.
48 C. Tian, B. Li, Y. Rui, H. Xiong, Y. Zhao, X. Han, X. Zhou, Y. Qiu, W. An, K. Li, *Adv. Funct. Mater.* **2023**, *33*, 2302270.
49 H. Xie, Z. Wang, Z. Chen, C. Pereyra, M. Pols, K. Gałkowski, M. Anaya, S. Fu, X. Jia, P. Tang, D. J. Kubicki, A. Agarwalla, H.-S. Kim, D. Prochowicz, X. Borrisé, M. Bonn, C. Bao, X. Sun, S. M. Zakeeruddin, L. Emsley, J. Arbiol, F. Gao, F. Fu, H. I. Wang, K.-J. Tielrooij, S. D. Stranks, S. Tao, M. Grätzel, A. Hagfeldt, M. Lira-Cantu, *Joule* **2021**, *5*, 1246-1266.
50 K. Wang, Z. Xu, Z. Guo, H. Wang, S. M. Qaid, K. Yang, Z. Zang, *Adv. Energy Mater*. **2024**, *14*, 2402249.
51 P. Mariani, M. Á. Molina-García, J. Barichello, M. Isabella Zappia, E. Magliano, L. A. Castriotta, L. Gabatel, S. B. Thorat, A. E. Del Rio Castillo, F. Drago, E. Leonardi, S. Pescetelli, L. Vesce, F. Di Giacomo, F. Matteocci, A. Agresti, N. De Giorgi, S. Bellani, A. Di Carlo, F. Bonaccorso, *Nat. Commun.* **2024**, *15*, 4552.
52 Y. Wang, I. Ahmad, T. L. Leung, J. Y. Lin, W. Chen, F. Z. Liu, A. M. C. Ng, Y. Zhang, A. B. Djurišić, *ACS Mater. Au* **2022**, *2*, 215−236.
53 F. Ren, Q. Lu, X. Meng, J. Zhou, R. Chen, J. Wang, H. Wang, S. Liu, Z. Liu, W. Chen, J. Energy Chem. 2024, 94, 1–9.
54 Qi Jiang1, Robert Tirawat1, Ross A. Kerner1, E. Ashley Gaulding2, Yeming Xian3, Xiaoming Wang3, Jimmy M. Newkirk, Y. Yan, J. J. Berry, K. Zhu, *Nature* **2023**, *623*, 313-318.
55 J. W. Schall, A. Glaws, N. Y. Doumon, T. J. Silverman, M. Owen-Bellini, Kent Terwilliger, Md A. Uddin, P. Rana, J. J. Berry, J. Huang, L. T. Schelhas, D. B. Kern, *Sol. RRL* **2023**, *7*, 2300229.
56 U. Erdil, M. Khenkin, W. M. B. de Araujo, Q. Emery, I. Lauermann, V. Paraskeva, M. Norton, S. Vediappan, D. K. Kumar, R. K. Gupta, I. Visoly-Fisher, M. Hadjipanayi, G. E. Georghiou, R. Schlatmann, A. Abate, E. A. Katz, C. Ulbrich, *Energy Technol.* **2025**, *13*, 2401280.
57 A. Levtchenko, A. Julien, D. McDermott, J. B. Puel, J. F. Guillemoles, D.Ory, D. Suchet, *Sol. RRL* **2024**, *8*, 2400511.
58 I. L. Repins, M. Owen-Bellini, M. D. Kempe, M. G. Deceglie, J. J. Berry, N. Y. Doumon, T. J. Silverman and L. T. Schelhas, Cell Rep. Phys. Sci. **2024**, *5*, 101969.
59 Z. L. Ren, J. Ovčar, T. L. Leung, Y. L. He, Y. Li, D. Y. Li, X. S. Qin, H. B. Mo, Z. T. Yuan, J. M. Bing, M. P. Bucknall, L. Grisanti, M. U. Ali, P. Bai, T. Zhu, A. A. Syed, J. Y. Lin, J. B. Wang, A. Khaleed,1 W. T. Sun, G. Y. Li, G. Li, A. M. C. Ng, A. W.Y. Ho-Baillie, I. Lončarić, J. Popović, A. B. Djurišić, *Matter* **2025**, *8*, 101937.
60 L. Chen, Y. Y. Tan, Z. X. Chen, T. Wang, S. Hu, Z. A. Nan, L. Q. Xie, Y. Hui, J. X. Huang, C. Zhan, S. H. Wang, J. Z. Zhou, J. W. Yan, B.W. Mao, Z. Q. Tian, *J. Am. Chem. Soc*. **2019**, *141*, 1665-1671.
61 C. C. Stoumpos, C. D. Malliakas, M. G. Kanatzidis, *Inorg. Chem.* **2013**, *52*, 9019−9038.
62 S. Min, M. Jeon, J. Cho, J. H. Bang and P. V. Kamat, Nano Convergence, 2024, 11, 49.
63 Z. J. Xu, R. A. Kerner, L. Kronik, B. P. Rand, *ACS Energy Lett.* **2024**, *9*, 4645−4654.
64 L. Yan, H. Huang, P. Cui, S. Du, Z. Lan, Y. Yang, S. Qu, X. Wang, Q. Zhang and B. Liu, *Nat. Energy* **2023**, *8*, 1158-1167.
65 R. Ahmed, S. Rehman, Z. Chen, F. Ye and X. Ren, *Angew. Chem. Int. Ed.* **2025**, *64*, e202418763.
66 M. Vásquez-Montoya, J. F. Montoya, D. Ramirez and F. Jaramillo, *J. Energy Chem.* **2021**, *57*, 386-391.

67 E. V. Péan, S. Dimitrov, C. S. De Castro, M. L. Davies, *Phys. Chem. Chem. Phys.* **2020**, *22*, 28345-28358.
68 X. Chen, P. V. Kamat, C. Janáky, G. F. Samu, *ACS Energy Lett.* **2024**, *9,* 3187-3203.
69 J. Thiesbrummel, S. Shah, E. Gutierrez-Partida, F. Zu, F. Peña-Camargo, S. Zeiske, J. Diekmann, F. Ye, K. P. Peters and K. O. Brinkmann, *Nat. Energy*, **2024**, *9*, 664-676.
70 R. T. Ginting, M.-K. Jeon, K.-J. Lee, W.-Y. Jin, T.-W. Kim and J.-W. Kang, *J. Mater. Chem. A*, **2017**, *5*, 4527-4534.
71 K. Domanski, B. Roose, T. Matsui, M. Saliba, S.-H. Turren-Cruz, J.-P. Correa-Baena, C. R. Carmona, G. Richardson, J. M. Foster and F. De Angelis, *Energy Environ. Sci.* **2017**, *10*, 604-613.